PHYSICAL REVIEW C **93**, 051303(R) (2016)

Nuclear charge and neutron radii and nuclear matter: Trend analysis in Skyrme density-functional-theory approach

P.-G. Reinhard[1] and W. Nazarewicz[2,3]

[1]*Institut für Theoretische Physik, Universität Erlangen, D-91054 Erlangen, Germany*

[2]*Department of Physics and Astronomy and FRIB Laboratory, Michigan State University, East Lansing, Michigan 48824, USA*

[3]*Institute of Theoretical Physics, Faculty of Physics, University of Warsaw, Warsaw, Poland*

(Received 23 January 2016; published 20 May 2016)

Background: Radii of charge and neutron distributions are fundamental nuclear properties. They depend on both nuclear interaction parameters related to the equation of state of infinite nuclear matter and on quantal shell effects, which are strongly impacted by the presence of nuclear surface.

Purpose: In this work, by studying the correlation of charge and neutron radii, and neutron skin, with nuclear matter parameters, we assess different mechanisms that drive nuclear sizes.

Method: We apply nuclear density functional theory using a family of Skyrme functionals obtained by means of optimization protocols, which do not include any radius information. By performing the Monte Carlo sampling of reasonable functionals around the optimal parametrization, we scan all correlations between nuclear matter properties and observables characterizing charge and neutron distributions of spherical closed-shell nuclei ^{48}Ca, ^{208}Pb, and ^{298}Fl.

Results: By considering the influence of various nuclear matter properties on charge and neutron radii in a multidimensional parameter space of Skyrme functionals, we demonstrate the existence of two strong relationships: (i) between the nuclear charge radii and the saturation density of symmetric nuclear matter ρ_0, and (ii) between the neutron skins and the slope of the symmetry energy L. The impact of other nuclear matter properties on nuclear radii is weak or nonexistent. For functionals optimized to experimental binding energies only, proton and neutron radii are found to be weakly correlated due to canceling trends from different nuclear matter characteristics.

Conclusion: The existence of only two strong relations connecting nuclear radii with nuclear matter properties has important consequences. First, by requiring that the nuclear functional reproduces the empirical saturation point of symmetric nuclear matter practically fixes the charge (or proton) radii, and vice versa. This explains the recent results of ab initio calculations with two-nucleon and three-nucleon forces optimized simultaneously to binding energies and radii of selected nuclei. Second, since the neutron skin uncertainty primarily depends on the slope of the symmetry energy, imposing constraints on *both* ρ_0 and L practically determines the nuclear size, modulo small variations due to shell effects.

DOI: 10.1103/PhysRevC.93.051303

Introduction. Radii of proton (or charge) and neutron distributions in atomic nuclei are key observables that can be directly related to fundamental properties of nuclear matter and to the nature of nuclear force (see Ref. [1] and references quoted therein). In heavy nuclei, the excess of neutrons gives rise to a neutron skin, characterized by the neutron distribution extending beyond the proton distribution. The neutron skin has been found to correlate with a number of observables in finite nuclei and nuclear and neutron matter [2–23]; hence, it beautifully links finite nuclei with extended nuclear matter found, e.g., in neutron stars.

The goal of this study is to understand the relations between proton and neutron radii and neutron skins using nuclear density functional theory (DFT) [24], which is a tool of choice in microscopic studies of complex nuclei. In particular, we inspect the relations between nuclear matter parameters characterizing effective interactions, here represented by Skyrme energy density functionals (EDFs) adjusted to experimental data. We vary the optimization strategies to achieve unbiased comparison of proton and neutron radii. By means of the statistical covariance technique, we quantify the intricate relation between the proton and neutron radius and explain the recent results of a comparative study for ^{48}Ca [1].

The strategy. To explore the correlations among neutron radius, proton radius, and neutron skin, we use the tools of linear regression based on least squares (χ^2), which were adopted recently in the nuclear context in Refs. [11,25–35]. In particular, we use here analysis of covariances (statistical correlations) among observables, error propagation, and an exploration of χ^2 in the vicinity of the best fit. Our starting point is the parametrization SV-min [36] optimized to the pool of ground-state data. The corresponding set of fit observables had been carefully selected to include only nuclei which have very small correlation corrections [37] and thus can be described reliably within a standard single-reference nuclear DFT. Since the set of fit observables constraining SV-min contains also information on radii deduced from the charge form factor data [38,39], this makes this EDF parametrization less useful for the present study, whose objective is to explore correlations with charge radii. Indeed, one should not trust correlations for an observable which was included in the fit as the behavior of χ^2 in the direction of this observable is usually very rigid [34]. To provide sufficient leeway to explore

radii, the radius information should be excluded from the fit. Thus we consider here the SV-min set of fit observables, however, now excluding the data on radii. This leaves in the fit pool only energy information, namely binding energies of 60 semimagic nuclei, pairing gaps from odd-even binding energy differences for long isotopic and isotonic chains, and a few selected spin-orbit splitting in doubly magic nuclei. (For details of the fit data, see Tables III and IV of Ref. [36].) The EDF optimized to this dataset is referred to as SV-E in the following. This parametrization and the effect of omission of radius information had been discussed in Refs. [31,35]. Here, we use SV-E particularly as a tool to explore radius correlations.

The Skyrme EDF is described by means of 14 parameters. The pairing functional contains three parameters: proton and neutron pairing strengths and a parameter defining the density dependence. Two parameters are used for calibrating the isoscalar and isovector spin-orbit force [40]. Two parameters are necessary to tune the surface energy. Finally, there remain seven parameters characterizing volume properties. These are fully equivalent to key properties of uniform symmetric nuclear matter at equilibrium, called henceforth nuclear matter parameters (NMP). Those are the saturation density ρ_0 and energy-per-nucleon E/A of symmetric nuclear matter; incompressibility K and effective mass m^*/m characterizing the isoscalar response; and symmetry energy J, slope of symmetry energy L, and Thomas-Reiche-Kuhn sum rule enhancement factor $\kappa_{\rm TRK}$ characterizing the isovector response. Those NMP will be used in the following to sort the results and establish correlations with radii. Table I shows the parameters of SV-min and SV-E together with their uncertainties.

For the following analysis, we employ three strategies. First, we employ the standard covariance analysis explained, e.g., in Refs. [29,41]. Here, we compute the covariance matrix for SV-E and use it to deduce the covariances (correlations) between the observables of interest. Second, we explore explicitly the hypersurface of reasonable parametrizations in the vicinity of the SV-E parameter set. Recall that around the minimum of χ^2 parametrizations are distributed with probability $W(\boldsymbol{p}) \propto \exp[\chi^2(\boldsymbol{p})]$ where $\boldsymbol{p}$ stands for the (14) free parameters of the model and $\boldsymbol{p_0}$ is the SV-E parameter set. We sample this distribution in a Monte Carlo fashion by representing it by an ensemble of 2000 parametrizations. Thereby, we confine the search to the space of $\boldsymbol{p}$ with $W(\boldsymbol{p}) > 1/2$ to avoid an excessive amount of unsuccessful hits in the large parameter space. The close vicinity of $\boldsymbol{p_0}$ suffices for the present purposes as it contains all crucial trends and correlations. (For more discussion of such strategy, see Ref. [30].) Finally, we employ the rules of error propagation in the context of χ^2 fits. We use this to explore the sensitivity of the radii to NMP by constraining the fit by selected NMP (while using always exactly the same pool of fit observables) and studying resulting changes in the uncertainties of the predicted radii. The chosen NMP is always fixed at the SV-E value. This means that the optimal parameters $\boldsymbol{p_0}$ remain the same. What changes are allowed variations in $\boldsymbol{p}$ which, in turn, impact the extrapolation uncertainties. We shall see a strong correlation if one NMP reduces significantly the uncertainty of an observable.

TABLE I. The parameters of SV-min and SV-E together with the correlated uncertainties. The NMP are shown in the upper block. The others are given for the form of the coupling constants as in Ref. [35]. We provide six significant figures for each parameter, although some of them would be sufficiently well defined with less digits. Note that the required precision of a parameter is much higher than the corresponding correlated uncertainty.

	SV-min		SV-E	
ρ_0 (MeV)	0.161085	±0.0011	0.154181	±0.0076
E/A (MeV)	−15.9099	±0.04	−15.8120	±0.17
K (MeV)	221.752	±8.1	273.733	±31.3
m^*/m	0.951806	±0.067	1.07038	±0.103
J (MeV)	30.6570	±1.9	27.2333	±2.4
L (MeV)	44.8138	±25.7	2.92329	±62.9
$\kappa_{\rm TRK}$	0.076522	±0.1919	0.192	±0.349
$C_0^{\Delta\rho}$ (MeV fm^5)	107.657	±6.6	85.39992	±10.7
$C_1^{\Delta\rho}$ (MeV fm^5)	−141.506	±162	−80.90533	±391
$C_0^{\nabla\mathbf{J}}$ (MeV fm^4)	−101.582	±5.5	−96.3170	±11.7
$C_1^{\nabla\mathbf{J}}$ (MeV fm^4)	−22.9681	±16.2	−21.5881	±18.2
$V_{\rm pair,p}$ (MeV fm^3)	601.160	±190	613.231	±209
$V_{\rm pair,n}$ (MeV fm^3)	567.190	±154	568.739	±173
$\rho_{0,\rm pair}$ (fm^{-3})	0.211591	±0.052	0.202513	±0.046

Results. We begin by inspecting in Fig. 1 the covariance matrices of SV-min and SV-E. The general pattern seen in Fig. 1 was discussed in Refs. [31,35]. The strong correlations between the isovector indicators (symmetry energy J, symmetry energy slope L, rms neutron radius $r_{\rm n}$, neutron skin $r_{\rm skin} = r_{\rm n} - r_{\rm p}$, and electric dipole polarizability $\alpha_{\rm D}$) seen in SV-min become significantly degraded in SV-E, with the strongest remaining correlation being that between $r_{\rm skin}$ and L. Indeed, as concluded in Refs. [31,35] L is the leading bulk parameter for isovector static response. The charge radius $r_{\rm ch}$ in SV-E correlates very well with the saturation point (ρ_0 and E/A) but rather poorly with other quantities, in particular with the neutron radius and neutron skin [8]. On the other hand, the neutron radius in SV-E has a reasonable correlation with $\alpha_{\rm D}$ but it is hardly correlated with $r_{\rm ch}$, ρ_0, and E/A. The lack of correlation between K and nuclear radii has been recognized in Refs. [8,42,43]. Therein, one also finds a weak correlation between ρ_0 and K, which is consistent with our results shown in Fig. 1.

In the following, we shall test the robustness of the correlations $r_{\rm ch} \leftrightarrow \rho_0$ and $r_{\rm skin} \leftrightarrow L$ by inspecting trends in ^{48}Ca, ^{208}Pb, and ^{298}Fl ($Z = 114, N = 184$), a spherical superheavy nucleus, in which the leptodermous expansion is expected to work best [44]. By considering a medium, heavy, and superheavy nucleus, we can assess whether finite-size (or shell) effects cloud our conclusions. To illustrate the impact of NMP on $r_{\rm ch}$ and $r_{\rm n}$, Fig. 2 shows the SV-E variance ellipsoids in the $(r_{\rm ch}, r_{\rm n})$ plane. Consistent with results displayed in Fig. 1, the variance ellipsoids are primarily impacted by the variations in the directions of ρ_0 and L. The impact of other NMP is much less. Interestingly, the directions of trends due to changes in ρ_0 and L (marked by arrows) are fairly different. That is, increasing ρ_0 decreases both $r_{\rm ch}$ and $r_{\rm n}$, as expected

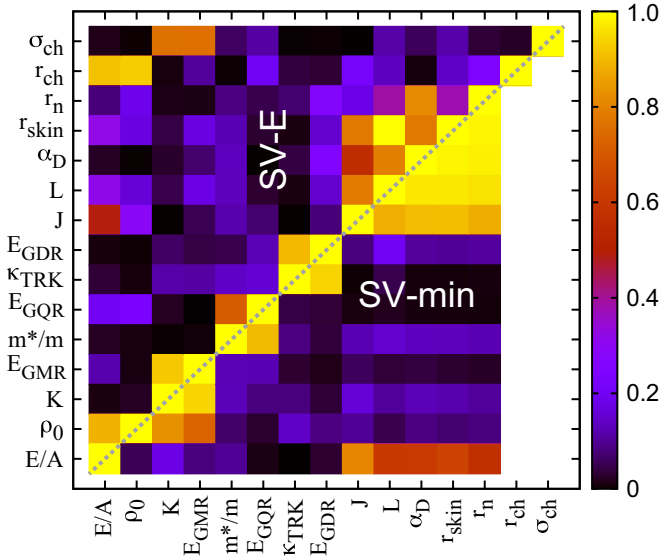

FIG. 1. Covariance matrices for a selection of observables and NMP computed with SV-min [36] (below the diagonal) and SV-E [31,35] (above the diagonal). Nuclear observables (in ^{208}Pb) are charge surface thickness $\sigma_{\rm ch}$; root-mean-square (rms) charge radius $r_{\rm ch}$; rms neutron radius $r_{\rm n}$; neutron skin $r_{\rm skin}$; electric dipole polarizability $\alpha_{\rm D}$; and giant resonance energies $E_{\rm GMR}$, $E_{\rm GDR}$, and $E_{\rm GQR}$. The NMP corresponding to the symmetric nuclear matter include incompressibility K, symmetry energy J, symmetry energy slope L, isoscalar effective mass m^*/m; TRK sum-rule enhancement $\kappa_{\rm TRK}$; and density ρ_0 and energy E/A at the saturation point. The correlations with the charge form factor data $\sigma_{\rm ch}$ and $r_{\rm ch}$ are not shown for SV-min as these quantities were included in the correspondins set of fit observables.

from the standard liquid-drop (or Fermi liquid theory) relation between the saturation density and the radius parameter (see Ref. [44] for more discussion). On the other hand, increasing L decreases $r_{\rm ch}$ and increases $r_{\rm n}$. The trend due to changes in J generally follows that of L, albeit with a much smaller magnitude. Due to the compensating trends, the correlation

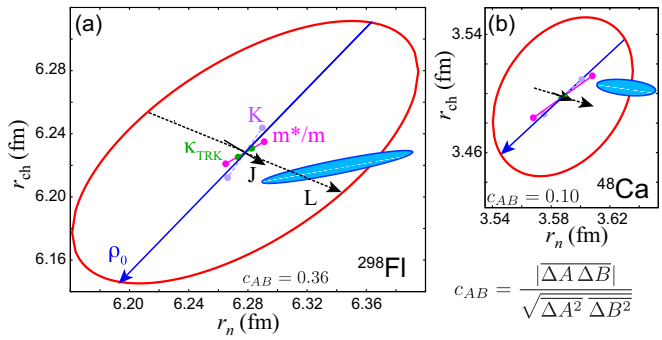

FIG. 2. Variance ellipsoids with SV-E in the ($r_{\rm ch}$,$r_{\rm n}$) plane for ^{298}Fl (a) and ^{48}Ca (b). The arrows and segments indicate the direction of changing radii when varying one NMP as indicated. Their lengths represent the magnitude of corresponding variations. The narrow ellipsoids mark the SV-min results. The correlation coefficient c_{AB} between $r_{\rm ch}$ and $r_{\rm n}$ is indicated in both cases.

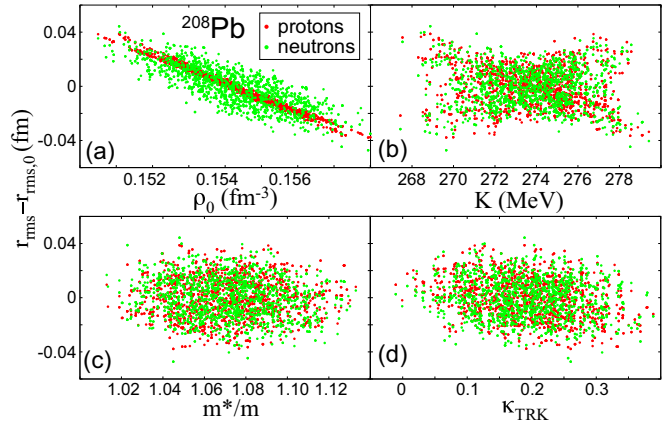

FIG. 3. Proton (red) and neutron (green) rms radii in ^{208}Pb with respect to the SV-E values from the ensemble of 2000 parametrizations in the vicinity of the optimal fit SV-E drawn vs different NMP: ρ_0 (a), K (b), m^*/m (c), and $\kappa_{\rm TRK}$ (d).

$r_{\rm ch} \leftrightarrow r_{\rm n}$ is very small; namely, it is $c_{AB} = 0.10$ for ^{48}Ca and it increases to $c_{AB} = 0.36$ for ^{298}Fl. This illustrates that these two quantities are not strongly coupled by the Skyrme EDF. Figure 2 also shows the corresponding SV-min ellipsoids (narrow, blue). As expected, these are very narrow in the direction of $r_{\rm ch}$, as this quantity has been constrained in the fit of SV-min. (It is interesting to note that the rms deviation from experimental data for $r_{\rm ch}$ are similar in SV-min (0.014 fm) and SV-E (0.012 fm).) On the other hand, the uncertainty in $r_{\rm n}$ is significant.

Figures 3–5 display systematic trends obtained with the ensemble of 2000 parametrizations around SV-E. These results fully confirm our previous findings. Namely, ρ_0, L, and J nicely correlate with rms radii and neutron skin while K,

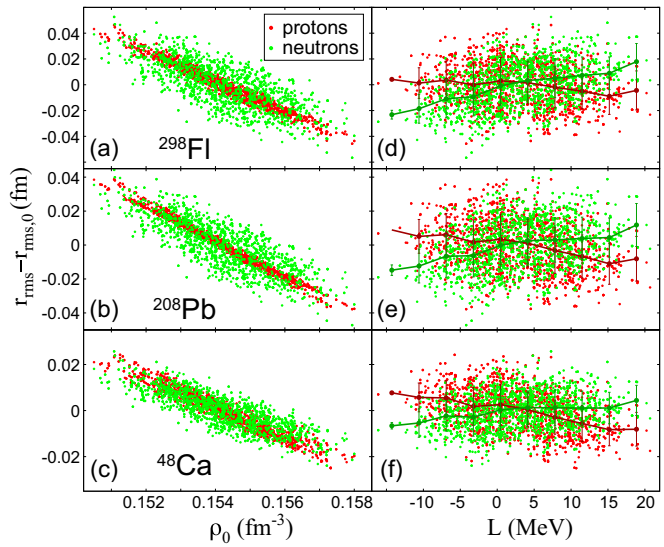

FIG. 4. Similar as in Fig. 3 but vs ρ_0 (left) and L (right) for ^{298}Fl (top), ^{208}Pb (middle), and ^{48}Ca (bottom). To illustrate the trends, the right panels show also averages and variances of radii taken over bins in L.

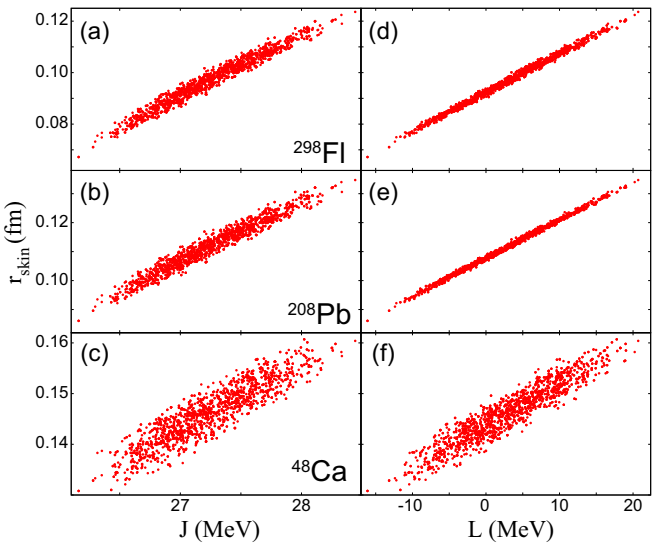

FIG. 5. Neutron skins from the ensemble of 2000 parametrizations in the vicinity of the optimal fit SV-E vs J (left) and L (right) for the three nuclei under consideration.

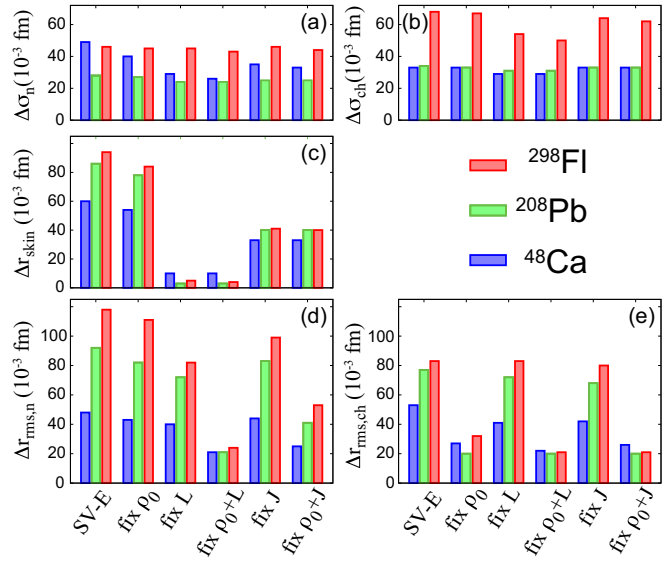

FIG. 6. Uncertainties in the predictions of rms neutron and charge radii (bottom), neutron skins (middle), and surface thicknesses (top) for different EDF fits. The reference EDF is SV-E. Other EDF fits use the same pool of fit observables as SV-E but constrain one or two NMP, as indicated, at the SV-E values.

m^*/m, and $\kappa_{\rm TRK}$ do not. The behavior of radii in Fig. 4 is consistent with the trends in Fig. 2 for the variance ellipsoids. It is interesting to notice that for a fixed value of ρ_0, the spread of the proton (or charge) radii is fairly narrow, while it is significantly broader for the neutron radii. Finally, as shown in Fig. 5, neutron skins correlate well with J but their correlation with L is superior, especially for heavy nuclei.

The strong $r_{\rm ch} \leftrightarrow \rho_0$ and $r_{\rm skin} \leftrightarrow L$ relations can be quantified by studying the predicted uncertainties on radii and skins. To this end, we carry out additional EDF optimizations by using the same pool of fit observables as SV-E but constraining one or two NMP at the values given by SV-E. Figure 6(e) illustrates the $r_{\rm ch} \leftrightarrow \rho_0$ correspondence: By constraining the saturation density ρ_0 the theoretical uncertainty on $r_{\rm ch}$ is reduced by $\sim 50\%$. Even more striking is the result for the neutron skin in Fig. 6(c): Constraining L in the EDF optimization practically fixes $r_{\rm skin}$. The correlation $r_{\rm skin} \leftrightarrow L$ follows from the leptodermous analysis [10], which shows that $r_{\rm skin} \propto L/J$.

The surface thickness parameters displayed in Figs. 6(a) and 6(b) are hardly affected by precise knowledge of ρ_0, L, and J. What about the neutron radii? As seen in Fig. 6(d), fixing ρ_0 or L helps reducing theoretical uncertainty slightly, but it is simultaneous knowledge of ρ_0 and L that helps reduce the error on $r_{\rm n}$. But this can be viewed as a secondary effect of the $r_{\rm ch} \leftrightarrow \rho_0$ and $r_{\rm skin} \leftrightarrow L$ relations. Indeed, $r_{\rm n} = r_{\rm p} + r_{\rm skin}$; hence, $\Delta r_{\rm n} = \Delta r_{\rm p} + \Delta r_{\rm skin}$. The uncertainty of the first term is reduced by precise information on ρ_0 while the error on the second term is reduced by our knowledge of L.

Figure 6 also shows results with EDFc obtained by constraining the symmetry energy J. As discussed earlier, the trends due to J follow those triggered by variations in L, but they are weaker. This is because our current knowledge of J is much better than that of L. For instance, as seen in Table I, the values of J are 31 ± 2 MeV in SV-min and 27 ± 2 MeV in SV-E (a mere 6–7% error), while the values of L in SV-min and SV-E are 45 ± 26 MeV and 3 ± 63 MeV, respectively (i.e., they are very uncertain).

Conclusion. By using the statistical tools of linear regression, we studied radii of neutron and proton distributions within the Skyrme-DFT framework. The analysis was carried out for the spherical closed-shell nuclei ^{48}Ca, ^{208}Pb, and ^{298}Fl, and the results turned out to weakly depend on the system considered, i.e., shell effects. Our statistical analysis has allowed us to explore various trends of charge and neutron radii with nuclear matter properties. The main conclusion of our study is that there exist, at least within the Skyrme-DFT theory, only two strong correlations. Namely, we found one-to-one relations between radii in finite nuclei and parameters ρ_0 and L characterizing the equation of state of uniform nuclear matter: $r_{\rm ch} \leftrightarrow \rho_0$ and $r_{\rm skin} \leftrightarrow L$. For instance, by including charge radii in a set of fit observables, as done for the majority of realistic Skyrme EDFs [24], one practically fixes the saturation density ρ_0. Indeed, as seen in Table I, by adding the charge form factor information to the set of fit observables of SV-E, one reduces the theoretical uncertainty on ρ_0 by a factor of 7 (from 0.0076 fm^{-3} in SV-E to 0.0011 fm^{-3} in SV-min). Recently, a similar conclusion has been reached in ab initio calculations based on a chiral interaction NNLO$_{\rm sat}$ optimized simultaneously to low-energy nucleon-nucleon scattering data, as well as binding energies and radii of finite nuclei [45]. Here, the use of data on charge radii was crucial for reproducing the empirical saturation point of symmetric nuclear matter. Interestingly, the relation $r_{\rm n} \leftrightarrow \rho_0$ is much weaker than that for $r_{\rm ch}$, so constraining the saturation density alone does not help significantly reducing the uncertainty on neutron (and mass) radii.

By inspecting various, often competing, trends in Fig. 2 one is tempted to conclude that the $r_n \leftrightarrow r_p$ relation is fairly complex. Namely, various trends are possible when moving along some trajectory in the parameter space $\{\boldsymbol{p}\}$. In this respect, we suggest the two directions that are most important are given by the variations in ρ_0 and L. Our analysis, in particular the results shown in Fig. 6, suggest that reducing the uncertainty on L would lead to a dramatic improvement in our knowledge of neutron skins and neutron radii. This is consistent with the findings of Ref. [18] that the slope of the symmetry energy L is the single main contributor to the statistical uncertainty of r_{skin}. Conversely, using the precise information on neutron skins (when available) should allow us to improve our knowledge of L and hence the neutron matter equation of state.

Finally, we conclude that while including experimental charge radii in the fit data gives rise to EDFs that constrain the saturation density ρ_0 rather well, the corresponding model uncertainties on the neutron radii due to our poor knowledge of L are still appreciable [18]. This explains the Skyrme-DFT results in a recent comparative study for ^{48}Ca [1].

Acknowledgments. This material is based upon work supported by the U.S. Department of Energy, Office of Science, Office of Nuclear Physics under Awards No. DE-SC0013365 (Michigan State University) and No. DE-SC0008511 (NUCLEI SciDAC-3 Collaboration); by the German Ministry of Science and Technology, Grant No. 05P12RFFTG; by the Deutsche Forschungsgemeinschaft, Grant No. RE 322-14/1; and by Bundesministerium für Bildung und Forschung (BMBF) under Contract No. 05P09RFFTB.

[1] G. Hagen, A. Ekström, C. Forssén, G. R. Jansen, W. Nazarewicz, T. Papenbrock, K. A. Wendt, S. Bacca, N. Barnea, B. Carlsson, C. Drischler, K. Hebeler, M. Hjorth-Jensen, M. Miorelli, G. Orlandini, A. Schwenk, and J. Simonis, Nat. Phys. **12**, 186 (2016).
[2] F. Tondeur, M. Brack, M. Farine, and J. Pearson, Nucl. Phys. A **420**, 297 (1984).
[3] P.-G. Reinhard, Nucl. Phys. A **649**, 305 (1999).
[4] B. Alex Brown, Phys. Rev. Lett. **85**, 5296 (2000).
[5] C. J. Horowitz and J. Piekarewicz, Phys. Rev. Lett. **86**, 5647 (2001).
[6] C. J. Horowitz and J. Piekarewicz, Phys. Rev. C **64**, 062802 (2001).
[7] S. Typel and B. A. Brown, Phys. Rev. C **64**, 027302 (2001).
[8] R. Furnstahl, Nucl. Phys. A **706**, 85 (2002).
[9] F. Sammarruca and P. Liu, Phys. Rev. C **79**, 057301 (2009).
[10] M. Centelles, X. Roca-Maza, X. Viñas, and M. Warda, Phys. Rev. Lett. **102**, 122502 (2009).
[11] P.-G. Reinhard and W. Nazarewicz, Phys. Rev. C **81**, 051303(R) (2010).
[12] X. Roca-Maza, M. Centelles, X. Viñas, and M. Warda, Phys. Rev. Lett. **106**, 252501 (2011).
[13] J. Piekarewicz, B. K. Agrawal, G. Colò, W. Nazarewicz, N. Paar, P.-G. Reinhard, X. Roca-Maza, and D. Vretenar, Phys. Rev. C **85**, 041302 (2012).
[14] B. K. Agrawal, J. N. De, and S. K. Samaddar, Phys. Rev. Lett. **109**, 262501 (2012).
[15] J. M. Lattimer and Y. Lim, Astrophys. J. **771**, 51 (2013).
[16] F. J. Fattoyev and J. Piekarewicz, Phys. Rev. Lett. **111**, 162501 (2013).
[17] W. Nazarewicz, P.-G. Reinhard, W. Satula, and D. Vretenar, Eur. Phys. J. A **50**, 20 (2014).
[18] M. Kortelainen, J. Erler, W. Nazarewicz, N. Birge, Y. Gao, and E. Olsen, Phys. Rev. C **88**, 031305(R) (2013).
[19] X. Roca-Maza, M. Brenna, B. K. Agrawal, P. F. Bortignon, G. Colò, L.-G. Cao, N. Paar, and D. Vretenar, Phys. Rev. C **87**, 034301 (2013).
[20] A. Meucci, M. Vorabbi, C. Giusti, and P. Finelli, Phys. Rev. C **90**, 027301 (2014).
[21] J. D. McDonnell, N. Schunck, D. Higdon, J. Sarich, S. M. Wild, and W. Nazarewicz, Phys. Rev. Lett. **114**, 122501 (2015).
[22] T. Inakura and H. Nakada, Phys. Rev. C **92**, 064302 (2015).
[23] C. Mondal, B. K. Agrawal, and J. N. De, Phys. Rev. C **92**, 024302 (2015).
[24] M. Bender, P.-H. Heenen, and P.-G. Reinhard, Rev. Mod. Phys. **75**, 121 (2003).
[25] F. J. Fattoyev and J. Piekarewicz, Phys. Rev. C **84**, 064302 (2011).
[26] P.-G. Reinhard and W. Nazarewicz, Phys. Rev. C **87**, 014324 (2013).
[27] P.-G. Reinhard, J. Piekarewicz, W. Nazarewicz, B. K. Agrawal, N. Paar, and X. Roca-Maza, Phys. Rev. C **88**, 034325 (2013).
[28] Y. Gao, J. Dobaczewski, M. Kortelainen, J. Toivanen, and D. Tarpanov, Phys. Rev. C **87**, 034324 (2013).
[29] J. Dobaczewski, W. Nazarewicz, and P.-G. Reinhard, J. Phys. G **41**, 074001 (2014).
[30] S. Goriely and R. Capote, Phys. Rev. C **89**, 054318 (2014).
[31] J. Erler and P.-G. Reinhard, J. Phys. G **42**, 034026 (2015).
[32] M. Kortelainen, J. Phys. G **42**, 034021 (2015).
[33] J. Piekarewicz, W.-C. Chen, and F. J. Fattoyev, J. Phys. G **42**, 034018 (2015).
[34] X. Roca-Maza, N. Paar, and G. Colò, J. Phys. G **42**, 034033 (2015).
[35] P.-G. Reinhard, Phys. Scr. **91**, 023002 (2015).
[36] P. Klüpfel, P.-G. Reinhard, T. J. Bürvenich, and J. A. Maruhn, Phys. Rev. C **79**, 034310 (2009).
[37] P. Klüpfel, J. Erler, P.-G. Reinhard, and J. A. Maruhn, Eur. Phys. J. A **37**, 343 (2008).
[38] J. Friedrich and N. Vögler, Nucl. Phys. A **373**, 192 (1982).
[39] J. Friedrich and P.-G. Reinhard, Phys. Rev. C **33**, 335 (1986).
[40] P.-G. Reinhard and H. Flocard, Nucl. Phys. A **584**, 467 (1995).
[41] S. Brandt, *Statistical and Computational Methods in Data Analysis* (Springer-Verlag, New York, 1997).
[42] J. Blaizot, J. Berger, J. Dechargé, and M. Girod, Nucl. Phys. A **591**, 435 (1995).
[43] S. Yoshida and H. Sagawa, Phys. Rev. C **69**, 024318 (2004).
[44] P.-G. Reinhard, M. Bender, W. Nazarewicz, and T. Vertse, Phys. Rev. C **73**, 014309 (2006).
[45] A. Ekström, G. R. Jansen, K. A. Wendt, G. Hagen, T. Papenbrock, B. D. Carlsson, C. Forssén, M. Hjorth-Jensen, P. Navrátil, and W. Nazarewicz, Phys. Rev. C **91**, 051301(R) (2015).